

Efficient Estimation of Barycentered Relative Time Delays for Distant Gravitational Wave Sources

Orion Sauter

Randall Lab, University of Michigan, 450 Church St., Ann Arbor MI 48109

E-mail: osauter@umich.edu

Vladimir Dergachev

Science Park Potsdam-Golm Am Mühlenberg 1 D-14476 Potsdam-Golm Germany

E-mail: vladimir.dergachev@aei.mpg.de

Keith Riles

Randall Lab, University of Michigan, 450 Church St., Ann Arbor MI 48109

E-mail: kriles@umich.edu

Abstract. Accurate determination of gravitational wave source parameters relies on transforming between the source and detector frames. All-sky searches for continuous wave sources are computationally expensive, in part, because of barycentering transformation of time delays to a solar system frame. This expense is exacerbated by the complicated modulation induced in signal templates. We investigate approximations for determining time delays of signals received by a gravitational wave detector with respect to the solar system barycenter. A highly non-linear conventional computation is transformed into one that has a pure linear sum in its innermost loop.

Keywords: LIGO, Gravitational Waves, Solar System Modeling Submitted to: *Class.*

Quantum Grav.

1. Introduction

The LIGO Continuous Wave (CW) group searches for gravitational waves from spinning neutron stars. Some searches target known pulsars, such as the Crab Pulsar, but other all-sky searches look for unknown sources over a broad frequency band. These searches require substantial computational resources, so any reduction in computational demands is helpful. In this paper, we examine one aspect of the searches amenable to simplification: calculation of signal time delays received by a gravitational wave detector

with respect to the solar system barycenter for an ensemble of assumed source sky positions[‡].

The LIGO Analysis Library[2] (LAL) used in many gravitational wave searches includes two methods used to orient detectors, signals, and sources in space and time: *LALBarycenterEarth* gives the Earth’s position in the International Celestial Reference Frame[3] (equivalent to J2000), with respect to the Solar System Barycenter.

LALBarycenter locates the detectors on Earth, and calculates the time a received signal would have been emitted by a wave source given the signal detection time and the source’s direction and distance, and taking into account effects such as Shapiro and Roemer Delays. These programs[4] have been checked by comparison with the widely used radio astronomy timing package, tempo[5, 6].

While the calculations performed by these methods are precise and reasonably fast, calling these routines for each time step and sky point searched can be costly. The search algorithm used by the authors is PowerFlux, a “quick-look” pipeline designed for all-sky searches[7]. PowerFlux, in its semi-coherent and loosely coherent modes[8], requires less precision than what the LALBarycenter routines provide. To speed calculation, therefore, we investigate approximate models for time delays, characterized here by “emission time”, the inferred time of signal emission in the solar system barycenter frame for a given signal reception time at the detector and distance to the source.

The analysis of barycenter timing corrections for the Earth-Sun system serves as a good example for a general circularized binary with small modulation depth. As the modulations of source and detector add independently, such an analysis could, in principle, be applied to a binary source simply by doubling the number of terms for an assumed model.

2. Mathematical model

The emission time T is a function of detector local time t , source location u and intrinsic source parameters p (for non-isolated neutron star). Because modern computer architectures are vector-based it is typically more efficient to compute arrays of values of $T(t, u, p)$ for sets of times $\mathcal{T} = \{t_i\}$ and templates $S = \{(u_j, p_j)\}$.

For a single template (u_0, p_0) the function $T(t, u_0, p_0)$ has a very non-trivial behaviour with several almost periodic influences from Sun, planets and the Moon as well as contributions from general relativity.

Because any analysis method must overlap templates (u, p) closely enough to provide sufficient coverage we can expect to compute arrays $T(\mathcal{T}, u, p)$ for nearby (u, p) .

Therefore, we separate the problem into two parts:

- Computation of $T(\mathcal{T}, u_0, p_0)$ for a fixed template (u_0, p_0) .
- Computation of differences $\Delta(\mathcal{T}, u, p) = T(\mathcal{T}, u, p) - T(\mathcal{T}, u_0, p_0)$

[‡] See ref. [1] for a recent study exploiting reduced order modeling of barycentering for targeted searches

When sets \mathcal{T} and S are finite we know that there exists the following decomposition:

$$\Delta(t_i, u_j, p_j) = \sum_{k=1}^N f_k(t_i) g_k(u_j, p_j) \quad (1)$$

where $f_k(t_i)$ and $g_k(u_j, p_j)$ are, in general, arbitrary 1-dimensional functions.

The key to our approach is that it is possible to find an approximate version of equation 1 with a number of terms N much smaller than the dimensionality of space spanned by $\Delta(t_i, u_j, p_j)$.

Besides providing computational efficiency this analysis identifies analytical functions f_k and g_k , paving the way for developing advanced *Loosely Coherent* [8, 9] semi-analytic statistics.

3. Prototype implementation

Typically, an individual PowerFlux search job is run over a small patch of sky, using Fourier transforms of 30 minutes or longer. If we compute a precise emission time for the center of the patch at each time needed, then we can consider other points as rotations from this center, and can fit the differences in emission time to a parameterized model. An example is shown in Figure 1. The fits use a total of 343 independent variables, which sets the minimum number of samples needed. Additional points add to the accuracy of both the fit, and the error estimation. We use the following procedure:

- (i) Divide the entire sky into a grid with 31 evenly-spaced rows of declination (δ), and 61 columns of right ascension (α). Add to these a set of points bordering the sun at angles between 0.005 radians and 0.00232 radians (5 times the solar radius). Exclude any of the grid points that fell within 0.00232 radians of the sun. The maximum distance between an arbitrary point and a grid point is 0.0517 radians.
- (ii) Divide the span of the first Advanced LIGO data run (O1) into segments of 250,000 second duration, overlapping the neighboring segments by 50,000 seconds each, defining a set of points and times spaced at 1-hour intervals for each segment.
- (iii) For each set, compute precise emission times at all skypoints and times.
- (iv) Shift all points in right ascension and/or declination by small angles for each 1-hour time interval
- (v) Compute precise emission times at each new point for the set.
- (vi) Compute the difference in emission times for each rotated and unrotated point at each time.

The shift is performed for $\Delta\alpha \in [-0.01, 0.01]$ radians and $\Delta\delta \in [-0.01, 0.01]$ radians, with 7 equally spaced values in each, for 49 possibilities. For each combination of shifts, 15,306 random locations and times are chosen from the original set. These are joined, to create a set of 7.5×10^5 points, and used as the input to the fit.

The points removed to avoid effects from the sun account for only a small fraction of the sky. The total area removed is 0.00170 radians², or 0.00859% of the sky. For a 0.01×0.01 radian patch, the maximum time that must be excluded is approximately 37 hours, or 1.68% of O1.

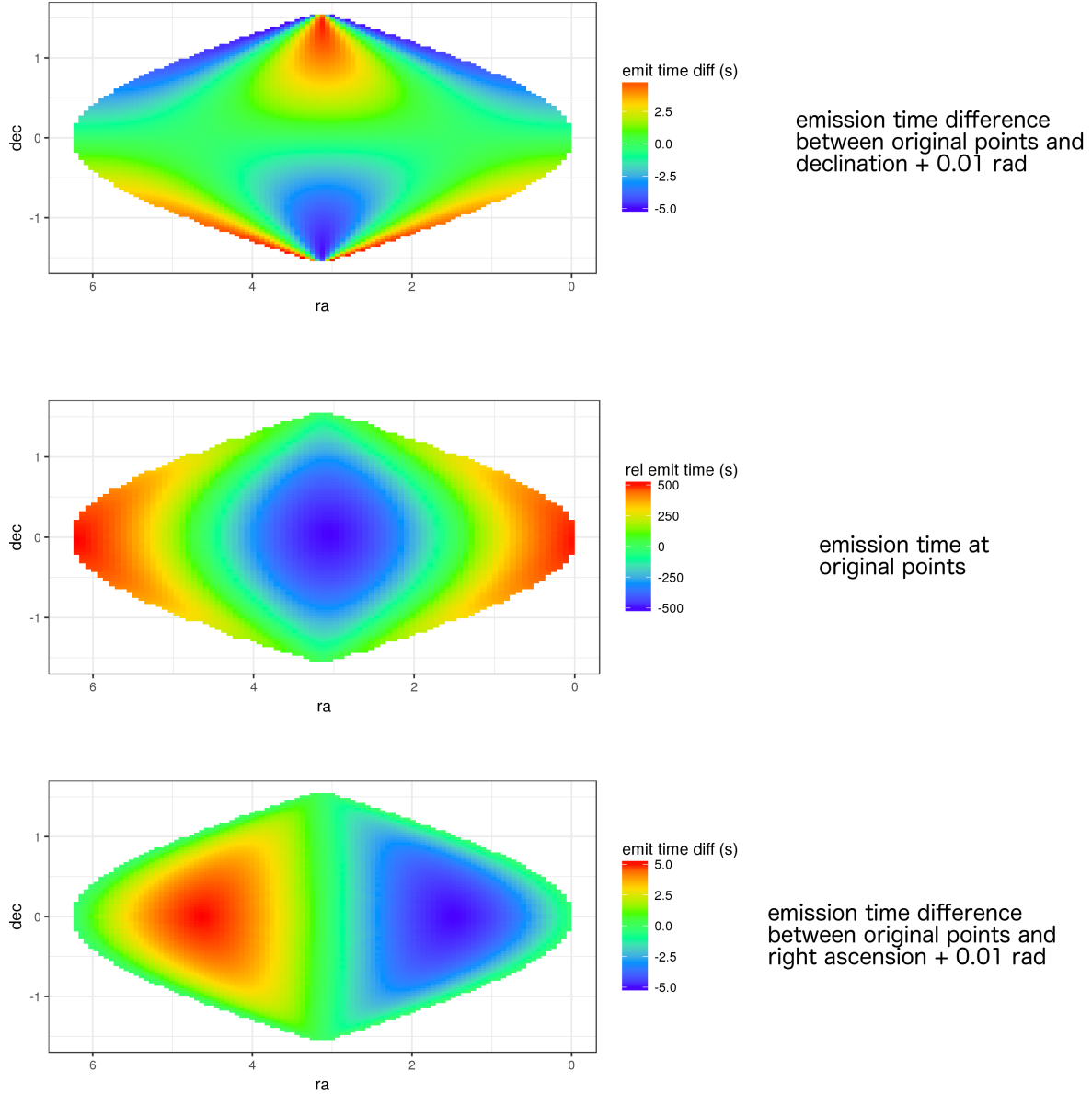


Figure 1. Example of emission time variation with sky position. Middle plot shows difference between computed emission time and time in local detector frame. Top plot shows difference in emission times between points offset in declination by 0.01 rad, while bottom plot shows difference in emission times between points offset in right ascension by 0.01 rad. Note that the color scales for difference plots are greatly reduced.

The fits to the difference in emission time are linear models, minimizing the sum of the squared errors. Ideally, the fits would minimize maximum absolute error, but the computational costs of such a routine proved too high. The terms use the following

parameters:

$$\begin{aligned}
e_1 &= \cos(\delta) \cos(\alpha) & \tilde{e}_1 &= \cos(\delta + \Delta\delta) \cos(\alpha + \Delta\alpha) \\
e_2 &= \cos(\delta) \sin(\alpha) & \tilde{e}_2 &= \cos(\delta + \Delta\delta) \sin(\alpha + \Delta\alpha) \\
e_3 &= \sin(\delta) & \tilde{e}_3 &= \sin(\delta + \Delta\delta)
\end{aligned} \tag{2}$$

The terms used are

- First- and second-order combinations of sine/cosine of right ascension/declination:

$$\begin{aligned}
&\sin(\alpha) && \cos(\delta) \sin(\alpha) \\
&\cos(\alpha) && \cos(\alpha) \cos(\alpha) \\
&\sin(\delta) && \sin(\delta) \cos(\alpha) \\
&\cos(\delta) && \cos(\delta) \cos(\alpha) \\
&\sin(\alpha) \sin(\alpha) && \sin(\delta) \sin(\delta) \\
&\cos(\alpha) \sin(\alpha) && \cos(\delta) \sin(\delta) \\
&\sin(\delta) \sin(\alpha) && \cos(\delta) \cos(\delta)
\end{aligned} \tag{3}$$

- Difference in rotated and original sky directions:

$$(\tilde{e}_1 - e_1) \quad (\tilde{e}_2 - e_2) \quad (\tilde{e}_3 - e_3) \tag{4}$$

- Scalar product of sky direction and ecliptic pole
- Products of sky direction difference and Δt :

$$\Delta t(\tilde{e}_1 - e_1) \quad \Delta t(\tilde{e}_2 - e_2) \quad \Delta t(\tilde{e}_3 - e_3) \tag{5}$$

- Products of Earth-Sun vector (in units of light-seconds), $\vec{\mathcal{S}}$, and direction difference:

$$\mathcal{S}_1(\tilde{e}_1 - e_1) \quad \mathcal{S}_2(\tilde{e}_2 - e_2) \quad \mathcal{S}_3(\tilde{e}_3 - e_3) \tag{6}$$

- Products of detector velocity vector (in units of c), \vec{v} , and direction difference:

$$\begin{aligned}
&v_1(\tilde{e}_1 - e_1) \\
&v_2(\tilde{e}_2 - e_2) \\
&v_3(\tilde{e}_3 - e_3)
\end{aligned} \tag{7}$$

- Products of sidereal-day sinusoids and second-order celestial sinusoids:

$$\begin{aligned}
&\sin(\Omega_{\text{Earth}} \Delta t) \sin(\alpha) \sin(\alpha) && \sin(\Omega_{\text{Earth}} \Delta t) \sin(\delta) \cos(\alpha) \\
&\cos(\Omega_{\text{Earth}} \Delta t) \sin(\alpha) \sin(\alpha) && \cos(\Omega_{\text{Earth}} \Delta t) \sin(\delta) \cos(\alpha) \\
&\sin(\Omega_{\text{Earth}} \Delta t) \cos(\alpha) \sin(\alpha) && \sin(\Omega_{\text{Earth}} \Delta t) \cos(\delta) \cos(\alpha) \\
&\cos(\Omega_{\text{Earth}} \Delta t) \cos(\alpha) \sin(\alpha) && \cos(\Omega_{\text{Earth}} \Delta t) \cos(\delta) \cos(\alpha) \\
&\sin(\Omega_{\text{Earth}} \Delta t) \sin(\delta) \sin(\alpha) && \sin(\Omega_{\text{Earth}} \Delta t) \sin(\delta) \sin(\delta) \\
&\cos(\Omega_{\text{Earth}} \Delta t) \sin(\delta) \sin(\alpha) && \cos(\Omega_{\text{Earth}} \Delta t) \sin(\delta) \sin(\delta) \\
&\sin(\Omega_{\text{Earth}} \Delta t) \cos(\delta) \sin(\alpha) && \sin(\Omega_{\text{Earth}} \Delta t) \cos(\delta) \sin(\delta) \\
&\cos(\Omega_{\text{Earth}} \Delta t) \cos(\delta) \sin(\alpha) && \cos(\Omega_{\text{Earth}} \Delta t) \cos(\delta) \sin(\delta) \\
&\sin(\Omega_{\text{Earth}} \Delta t) \cos(\alpha) \cos(\alpha) && \sin(\Omega_{\text{Earth}} \Delta t) \cos(\delta) \cos(\delta) \\
&\cos(\Omega_{\text{Earth}} \Delta t) \cos(\alpha) \cos(\alpha) && \cos(\Omega_{\text{Earth}} \Delta t) \cos(\delta) \cos(\delta)
\end{aligned} \tag{8}$$

here $\Omega_{\text{Earth}} = 2\pi/\text{sidereal day}$.

- Products of $(\Delta t)^2$ and second-order celestial sinusoids:

$$\begin{aligned} & \Delta t^2 \sin(\alpha) \sin(\alpha) & \Delta t^2 \sin(\delta) \cos(\alpha) \\ & \Delta t^2 \cos(\alpha) \sin(\alpha) & \Delta t^2 \cos(\delta) \cos(\alpha) \\ & \Delta t^2 \sin(\delta) \sin(\alpha) & \Delta t^2 \sin(\delta) \sin(\delta) \\ & \Delta t^2 \cos(\delta) \sin(\alpha) & \Delta t^2 \cos(\delta) \sin(\delta) \\ & \Delta t^2 \cos(\alpha) \cos(\alpha) & \Delta t^2 \cos(\delta) \cos(\delta) \end{aligned} \quad (9)$$

- Products of sky direction and Earth-Sun vector:

$$e_1 \mathcal{S}_1 \quad e_2 \mathcal{S}_2 \quad e_3 \mathcal{S}_3 \quad (10)$$

- Products of sky direction and detector velocity:

$$\begin{aligned} & v_1(\tilde{e}_1 - e_1) \\ & v_2(\tilde{e}_2 - e_2) \\ & v_3(\tilde{e}_3 - e_3) \end{aligned} \quad (11)$$

- Second-order combinations of Δt and $\cos(\delta)$:

$$\Delta t \cos(\delta) \quad \Delta t^2 \cos(\delta) \quad \Delta t \cos(\delta)^2 \quad (12)$$

- Terms accounting for Shapiro delay near sun:

$$\ln(1 - \tilde{\mathbf{e}} \cdot \vec{\mathcal{S}}) \quad 1/(1 - \tilde{\mathbf{e}} \cdot \vec{\mathcal{S}}) \quad (13)$$

Each of these terms is multiplied by $\Delta\alpha, \Delta\delta, \Delta\alpha^2, \Delta\delta^2, \Delta\alpha\Delta\delta$. In addition, we include terms

$$\Delta t(\tilde{e}_1 - e_1) \quad \Delta t(\tilde{e}_2 - e_2) \quad \Delta t(\tilde{e}_3 - e_3) \quad (14)$$

without $\Delta\alpha/\Delta\delta$ factors. Each term goes to zero when the rotation angle goes to zero. Note that sun-earth and detector velocity vectors are those for the saved points.

As an example, figure 2 shows the fit for gps time 1134233121, which has the largest maximum error among the fits, 1.59×10^{-5} s. The expression is a bilinear product of precomputed fit coefficients and monomials in $\Delta\alpha, \Delta\delta$ and Δt . In a practical implementation the grid of displacements, and thus monomial coefficients, is kept static inside the loop that computes Δt . The the actual computation of Δt easily vectorizes and takes few instructions on modern computers. Note that it is not necessary to keep the grid static with respect to all variables. For example, the grid can be static in $\Delta\delta$ and depend on t and α - the monomial grid recompute cost will be amortized away.

Results

As a maximum acceptable error, we chose a 30 degree phase difference for a 2 kHz signal, or 42 μs . The fit terms given above achieved this goal in the fitting set, but

$$\begin{aligned}
\Delta T = & [-10(\tilde{e}_1 - e_1) + 1.05(\tilde{e}_2 - e_2)]10^{-5} \Delta \mathbf{t} \\
& + [3210e_2 + 457e_1 + 307(\tilde{e}_1 - e_1) + 1310(\tilde{e}_2 - e_2) + 332(\tilde{e}_3 - e_3) - 0.156\mathcal{S}_1(\tilde{e}_1 - e_1) \\
& - 3.01\mathcal{S}_2(\tilde{e}_2 - e_2) - 1.68\mathcal{S}_3(\tilde{e}_3 - e_3) - 5480v_1(\tilde{e}_1 - e_1) - 1510000v_3(\tilde{e}_3 - e_3) \\
& - 0.00205e_1\mathcal{S}_1 - 7.22e_2\mathcal{S}_2 + 87600e_1v_1 - 4050000e_2v_2] \Delta \alpha \\
& + [-1.56(\tilde{e}_1 - e_1) + 3.14(\tilde{e}_2 - e_2) - 0.635(\tilde{e}_3 - e_3)]10^{-5} \Delta \alpha \Delta \mathbf{t} \\
& + [194 \cos(\delta) - 448e_3 \sin(\alpha) + 7.44e_2 - 60.3e_3 \cos(\alpha) - 0.845e_1 + 51(\tilde{e}_1 - e_1) \\
& - 18.2(\tilde{e}_2 - e_2) - 101(\tilde{e}_3 - e_3) - 0.872\mathcal{S}_1(\tilde{e}_1 - e_1) + 0.0412\mathcal{S}_2(\tilde{e}_2 - e_2) + 0.568\mathcal{S}_3(\tilde{e}_3 - e_3) \\
& - 2090000v_3(\tilde{e}_3 - e_3) + 0.000194e_1\mathcal{S}_1 - 0.0164e_2\mathcal{S}_2 - 8310e_1v_1 - 9210e_2v_2] \Delta \delta \\
& + [-8.75(\tilde{e}_1 - e_1) - 1.85(\tilde{e}_3 - e_3) + 0.456 \cos(\delta)]10^{-5} \Delta \delta \Delta \mathbf{t} \\
& + [1170e_2 + 237e_1 - 3570(\tilde{e}_1 - e_1) + 281(\tilde{e}_2 - e_2) + 990(\tilde{e}_3 - e_3) + 61.3\mathcal{S}_1(\tilde{e}_1 - e_1) \\
& - 0.461\mathcal{S}_2(\tilde{e}_2 - e_2) + 4.65\mathcal{S}_3(\tilde{e}_3 - e_3) - 4.15 \times 10^{08}v_3(\tilde{e}_3 - e_3) - 0.052e_1\mathcal{S}_1 \\
& - 2.42e_2\mathcal{S}_2 + 2220000e_1v_1 - 1360000e_2v_2] \Delta \alpha^2 \\
& + [2.53e_2 - 0.0879e_1] \Delta \alpha \sin(\Omega_{\oplus} \Delta \mathbf{t}) + [616(\tilde{e}_1 - e_1) - 338(\tilde{e}_3 - e_3)]10^{-5} \Delta \alpha^2 \Delta \mathbf{t} \\
& + [-3.5e_2 - 0.0636e_1] \cos(\Omega_{\oplus} \Delta \mathbf{t}) \Delta \alpha \\
& + [161e_2 + 187e_1 - 4750(\tilde{e}_1 - e_1) + 3880(\tilde{e}_3 - e_3) + 81.1\mathcal{S}_1(\tilde{e}_1 - e_1) - 0.156\mathcal{S}_2(\tilde{e}_2 - e_2) \\
& + 16.1\mathcal{S}_3(\tilde{e}_3 - e_3) - 1.54 \times 10^{09}v_3(\tilde{e}_3 - e_3) - 0.0499e_1\mathcal{S}_1 - 0.85e_2\mathcal{S}_2 - 0.5e_3\mathcal{S}_3 \\
& + 2130000e_1v_1 - 477000e_2v_2] \Delta \delta^2 \\
& + [0.0119e_3 \sin(\alpha) + 0.00578e_2 - 0.00845e_3 \cos(\alpha) + 0.00721e_1] \Delta \delta \sin(\Omega_{\oplus} \Delta \mathbf{t}) \\
& + [815(\tilde{e}_1 - e_1) - 1260(\tilde{e}_3 - e_3)]10^{-5} \Delta \delta^2 \Delta \mathbf{t} + [-0.669e_2 - 0.0954e_1]10^{-10} \Delta \alpha \Delta \mathbf{t}^2 \\
& + [0.00856e_3 \sin(\alpha) - 0.00799e_2 + 0.012e_3 \cos(\alpha) + 0.00521e_1] \cos(\Omega_{\oplus} \Delta \mathbf{t}) \Delta \delta \\
& + [0.855e_2 - 1.93e_1] \Delta \alpha^2 \sin(\Omega_{\oplus} \Delta \mathbf{t}) \\
& + [-0.0405 \cos(\delta) + 0.0935e_3 \sin(\alpha) - 0.00154e_2 + 0.00897e_3 \cos(\alpha)]10^{-10} \Delta \delta \Delta \mathbf{t}^2 \\
& + [-1.18e_2 - 1.39e_1] \cos(\Omega_{\oplus} \Delta \mathbf{t}) \Delta \alpha^2 + [-1.86e_1] \Delta \delta^2 \sin(\Omega_{\oplus} \Delta \mathbf{t}) \\
& + [-0.179e_2 - 0.326e_1]10^{-10} \Delta \alpha^2 \Delta \mathbf{t}^2 + [-1.33e_1] \cos(\Omega_{\oplus} \Delta \mathbf{t}) \Delta \delta^2 \\
& + [19.5e_3 \sin(\alpha) + 2460e_2 - 149e_3 \cos(\alpha) + 17.9e_1 + 139(\tilde{e}_1 - e_1) + 186(\tilde{e}_3 - e_3) \\
& - 2.39\mathcal{S}_1(\tilde{e}_1 - e_1) - 45100000v_3(\tilde{e}_3 - e_3) - 5.42e_2\mathcal{S}_2 + 176000e_1v_1 - 3040000e_2v_2] \Delta \delta \Delta \alpha \\
& + [-24(\tilde{e}_1 - e_1) - 36.6(\tilde{e}_3 - e_3) + 0.174 \cos(\delta)]10^{-5} \Delta \delta \Delta \alpha \Delta \mathbf{t} \\
& + [1.91e_2] \Delta \delta \Delta \alpha \sin(\Omega_{\oplus} \Delta \mathbf{t}) + [-2.64e_2] \cos(\Omega_{\oplus} \Delta \mathbf{t}) \Delta \delta \Delta \alpha \\
& + [-0.069 \cos(\delta) + 0.272e_3 \sin(\alpha) - 0.501e_2 + 0.0951e_3 \cos(\alpha)]10^{-10} \Delta \delta \Delta \alpha \Delta \mathbf{t}^2
\end{aligned}$$

Figure 2. Example of a fit for GPS time 1134233121. This fit has the largest error of 1.59×10^{-5} s. The expression is a bilinear product between precomputed fit coefficients and monomials in $\Delta \alpha$, $\Delta \delta$ and Δt . Only significant terms are shown.

we wished to test situations similar to those in which the model would be used. We chose $16 \times 8 = 128$ points on the sky, evenly spaced in right ascension and declination, to serve as patch centers. For each patch, we shifted the central point by a random value in $[-0.01, 0.01]$ for right ascension, and another for declination. A total of 50 shifted points were generated for each patch. We divided the span of the first Advanced LIGO data run (~ 4 months), O1, into 250,000 second chunks, overlapping by 50,000 seconds, and took time points from each chunk at 2,000-second intervals. We used LALBarycenter to obtain reference values for all points, then applied the fit model to each patch's points as a deflection from its center. A plot of the maximum absolute residual for each Δt and $\Delta\phi$ is shown in Figure 3. The maximum absolute residual for each reference time is shown in Figure 4. All points fell below the error threshold. We also show a histogram of all errors in Figure 5. The bulk of the errors are well below the threshold, and for a search of this length, any particular point would spend only a small fraction of time in a high-error region.

The *Loosely Coherent* method of detecting signals focuses on analysis of sets of potential templates. For the set based on nearby sky locations it is important to understand the evolution of signal phases for nearby templates. The fit described in this paper demonstrates that relatively few parameters are needed to describe time arrival differences between nearby templates.

This provides an efficient method to compute emission time corrections, provides a basis for extension of the PowerFlux cache to longer coherence times and lays the groundwork for future development of *Loosely Coherent* algorithms.

References

- [1] Pitkin M *et al.* Nov 2017 *Submitted to M.N.R.A.S.* arXiv:1711.08386
- [2] LIGO Scientific Collaboration LIGO Analysis Library Suite URL <https://wiki.ligo.org/DASWG/LALSuite>
- [3] Fey A L *et al.* 2015 *The Astronomical Journal* **150**
- [4] Abbott B *et al.* (LIGO Scientific Collaboration) 2004 *Phys. Rev. D* **69**(8) 082004
- [5] Edwards R T, Hobbs G B and Manchester R N URL www.atnf.csiro.au/research/pulsar/tempo
- [6] Edwards R T, Hobbs G B and Manchester R N 2006 *Monthly Notices of the Royal Astronomical Society* **372** 1549–1574
- [7] Abbott B P *et al.* 2008 *Phys. Rev. D* **77**
- [8] Dergachev V 2010 *Class. Quantum Grav.* **27**
- [9] Dergachev V 2012 *Phys. Rev. D* **85**

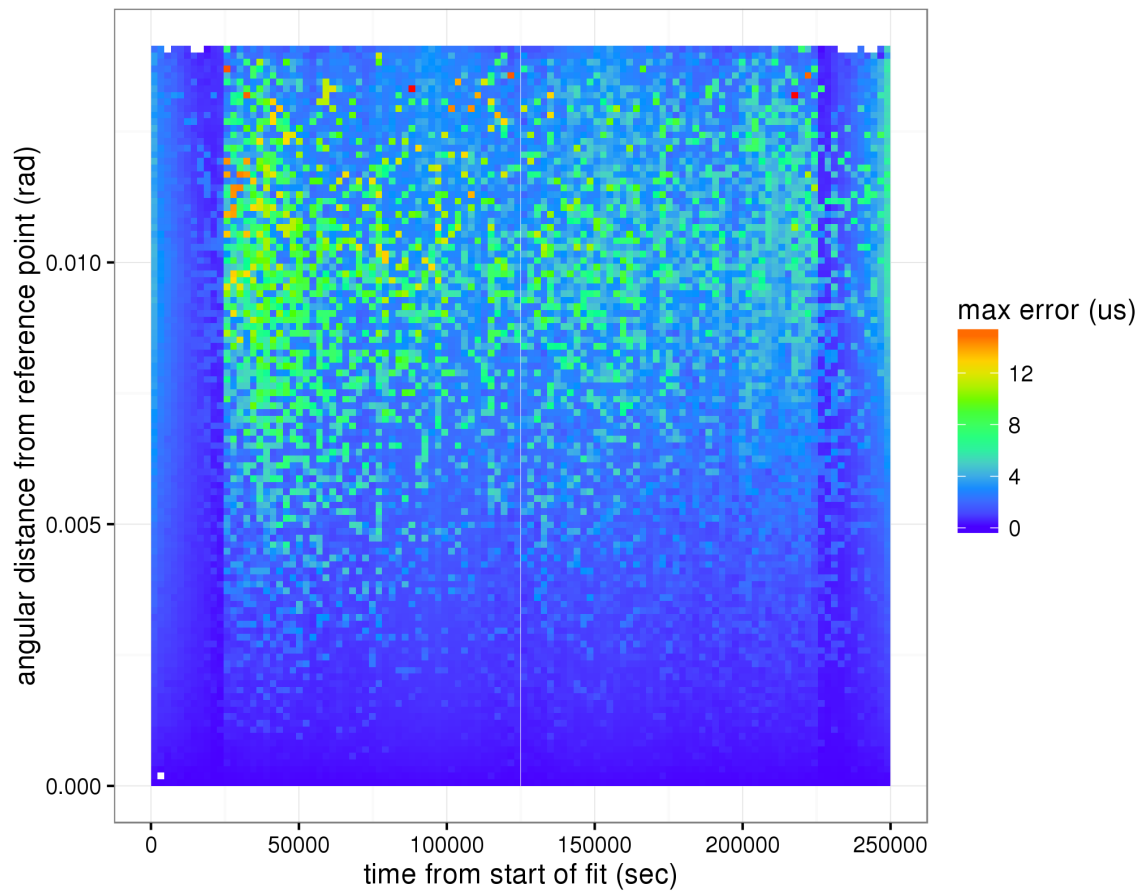


Figure 3. Maximum absolute residual over all test patches.

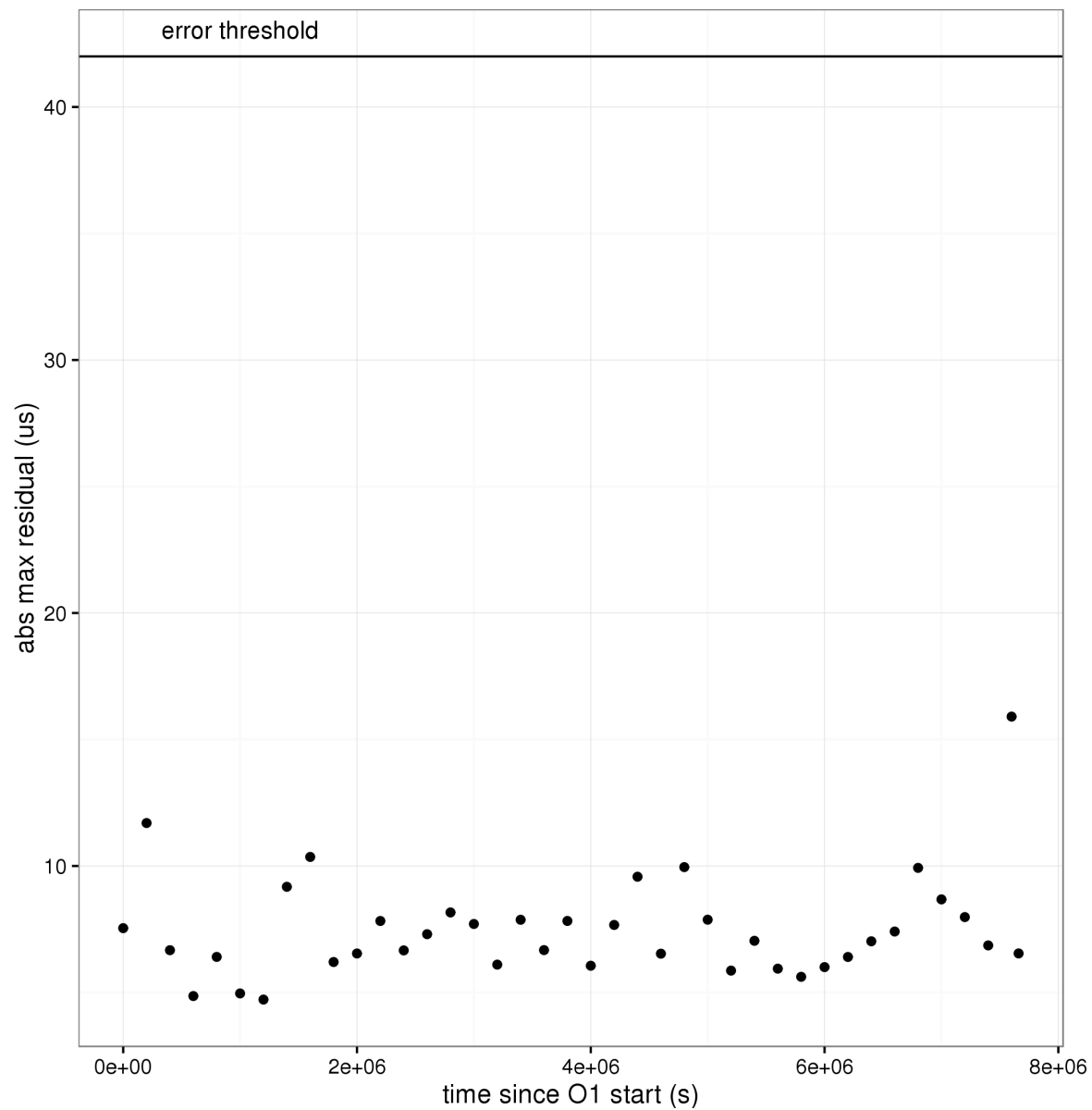


Figure 4. Maximum absolute residual for each fit.

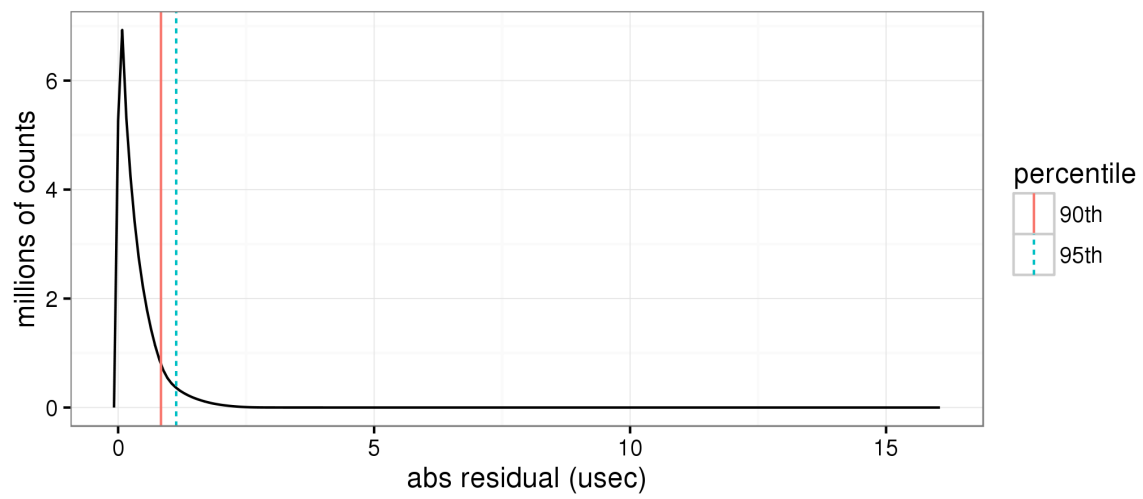


Figure 5. Distribution of residual magnitude. For large-timebase searches, only the bulk of the distribution matters, which is well below the error threshold.